PROCEEDINGS, 42nd Workshop on Geothermal Reservoir Engineering
Stanford University, Stanford, California, February 13-15, 2017
SGP-TR-212

Geothermometry of the Breitenbush Hot Springs Area, Oregon, USA

Donnel Malkemus, Robert B. Perkins, and Carl D. Palmer

Department of Geology, Portland State University, P.O. Box 751, Portland OR 97207

rperkins@pdx.edu

Keywords: Geothermometry, Geothermal, RTEst, Breitenbush, Oregon Cascades

ABSTRACT

Geothermometry of the Breitenbush Hot Springs area, located in the central Oregon Cascades, was studied to clarify previously reported reservoir temperatures of 129 to 202°C. Water samples collected from the Brietenbush Hot Springs area included springs (5), wells (8) and stream water samples (2) from the South Fork of the Breitenbush River. Geothermometry was interpreted using the Reservoir Temperature Estimator (RTEst) software package (Palmer, 2015) and constrained by reported mineralogy.

Optimized parameters were reservoir temperature and CO_2 fugacity. Water addition to account for steam formation was not used as initial runs indicated that inclusion as an optimization parameter led to large parameter uncertainties. Using RTEst with a chalcedony, mordenite-K, calcite, and heulandite mineral assemblage and deriving Al concentrations from assumed equilibrium with K-feldspar resulted in an average temperature estimate of 137 ±2 °C. This calculated reservoir temperature is significantly less than the 174 to 180 °C values reported in other multicomponent geothermometric studies (Forcella, 1982; Ingebritsen et al., 1992; Pang and Reed, 1998; Spycher et al., 2016). However, our new estimate shows promise in its consistency in estimated reservoir temperature, CO_2 fugacity (log(fCO2) = -0.06 ±0.07) and pH (6.04 ±0.06). In addition, calculated Al concentrations (9.6 ±0.5 ug/L) are consistent with the measured concentrations (8.9 ±4.6 ug/L). Most of the previously reported secondary minerals can be explained by equilibrium or supersaturated states obtained with this model. The estimated reservoir temperature is close to the reported maximum downhole temperature of 141 °C in a deep well located 3 km southeast of the hot springs. Thus, the proposed geothermometric model is consistent with mineralogical, aqueous geochemical, fluid inclusion data, and temperature observations near the site.

1. INTRODUCTION

Breitenbush Hot Springs is located in the central Oregon Cascades, approximately 15 kilometers northwest of Mount Jefferson, along the Breitenbush River (Figure 1). Geothermal interest in the Breitenbush area dates back to its original settlement in the late 1800s and the establishment of a hot spring resort in the early 20th century. The geothermal potential of Breitenbush has been the focus of several past studies that have included both classical and multi-component geothermometric assessments. In this paper, we provide a reassessment of the geothermometry of the area using a multicomponent optimization approach.

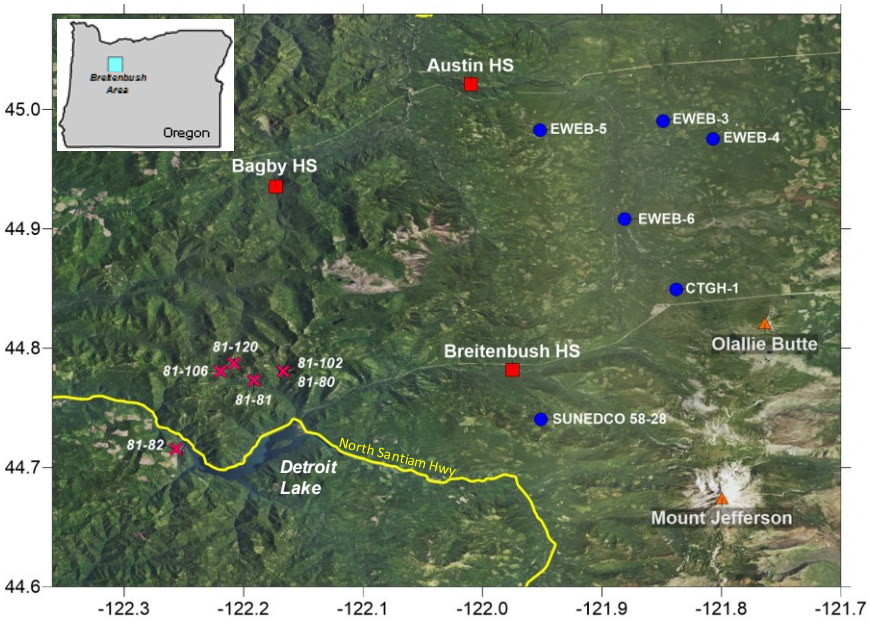

Figure 1. Breitenbush regional location map. The blue circles denote drill holes and the pink X denote outcrop samples.

2. SITE DESCRIPTION

2.1 Geological Setting

The Cascade Range in Oregon and Washington can be divided broadly into two major stratigraphic sections, both of which are related to arc volcanism associated with the subduction of the Juan de Fuca plate beneath the North American plate: the Western Cascades Group (WCG) and the High Cascades Group (HCG) (Hammond, 1979). The WCG is composed of a thick (5 to 8.5 km) section of volcanic and volcaniclastic rocks, generally older than 12 Ma (Hammond, 1979). In the Breitenbush area, the WCG consists of a diverse array of pyroclastic flows and lahars, basaltic to rhyodacitic lava flows, tuffaceous sandstones, and siltstones (Sherrod and Conrey, 1988). The Breitenbush Formation is the most significant and oldest WCG unit in the study area, being at least 2.5 km thick with an approximate age range of 25 to 18 Ma (Sherrod and Conrey, 1988). The HCG is composed of recent (about 5 Ma to present) andesitic and basaltic lava flows, with lesser pyroclastic flows (Hammond, 1979). Near the Breitenbush area, the HCG consists of "thick, stubby" andesite, dacite, and rhyodacite flows, generally higher in silica than other areas of the Cascades, the youngest of which is are recent flows at Mount Jefferson, approximately 15 km southeast of Breitenbush Hot Springs (Sherrod and Conrey, 1988).

The Breitenbush Formation is folded into a northeast plunging anticline associated with northwest-southeast crustal shortening that began approximately 18 Ma and ended by 12 Ma (Priest, 1990). The axis of the anticline is approximately 5 km northwest of Breitenbush Hot Springs (Sherrod and Conrey, 1988). The younger HCG volcanics unconformably overlie the anticline. Northwest trending faults present in a wide region of central and northern Oregon displace rocks older than middle Miocene. Fewer north- and northwest- trending faults, including several mapped in the vicinity of Breitenbush Hot Springs, displace Pliocene and younger rocks.

2.2 Geothermal Exploration and Characterization

In the 1970s and 80s, several investigations were conducted to assess geothermal potential of the Breitenbush Hot Springs area. The bulk of the results were published in a 1988 State of Oregon special report, from which the majority of this exploration history is summarized (Sherrod, 1988). Several geothermal exploration wells were installed in the vicinity of Breitenbush Hot Springs. In 1979, 4 temperature gradient holes (EWEB-3 through EWEB-6) were drilled close to the crest of the Cascades, approximately 15 to 20 km north-northeast of Breitenbush Hot Springs, through Miocene to Oligocene basaltic andesite to rhyodacite flows (Conrey and Sherrod, 1988). In 1981, a 2,457 meter deep well was drilled approximately 3 km southeast of Breitenbush Hot Springs (SUNEDCO 58-28 drill hole; Bargar, 1994) (Figure 1). Except for the upper ~100 meters, which extend through basalt and basaltic andesite flows, the entirety of the well was drilled through tuffs, tuffaceous sedimentary rocks, and occasional volcaniclastic deposits of the Breitenbush Formation (Bargar, 1994). In 1986, a 1,463-meter hole was advanced near Olallie Butte, approximately 10 km northeast of Breitenbush Hot Springs. The majority of the hole was drilled through basaltic andesite, with relatively minor intervals of basalt, dacite, and tuff (Conrey and Sherrod, 1988). In addition to these wells, several wells were drilled at the Breitenbush Hot Springs Resort for use as district heating and for filling soaking pools (Figure 2). Pertinent information such as depth, temperature, use, and approximate flow rates for each of the wells is summarized in Malkemus (2016).

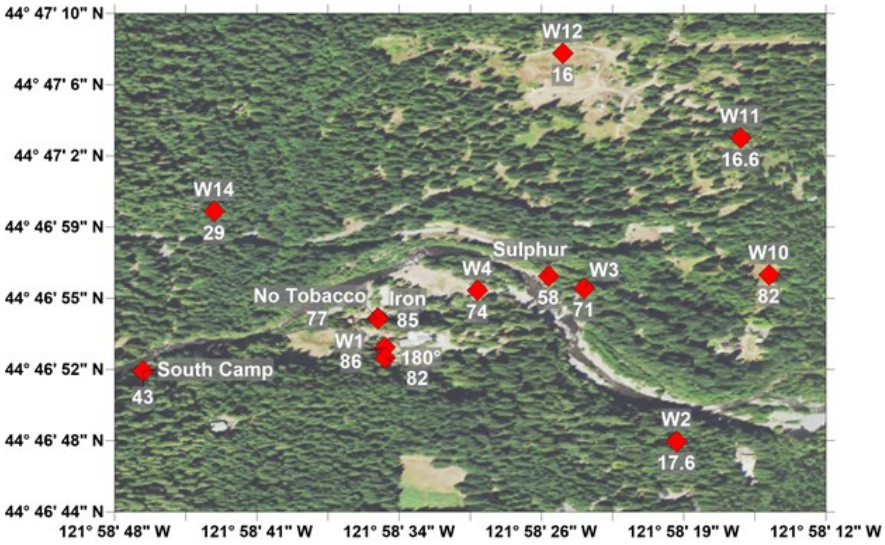

Figure 2. Well and spring locations at Breitenbush Hot Springs area. Numbers at each location denote the field measured outflow temperature in degrees Celsius. The "180°" designation is the name of one of the springs.

Characterization of alteration mineralogy present in the geothermal wells and in rocks exposed at the surface in the Breitenbush area showed higher temperature alteration at the center of the Breitenbush anticline and at depth in the SUNEDCO 58-28 drill hole when compared to the flanks of the anticline or in shallower portions of the well (Keith, 1988). The fact that shallower exposures of the oldest rock share alteration mineralogy with deeper rocks of the same age implies that the highest temperature alteration occurred prior to folding (i.e. before 18 to 12 Ma) (Keith, 1988). Shallower alteration mineralogy is limited to the zeolite-facies, with lower temperature zeolite-facies assemblages present at and near surface (Keith, 1988). Table 1 lists minerals identified in boreholes in the Breitenbush

area. Figure 3 shows the relative distribution of minerals in the SUNEDCO 58-28 drill hole with depth. These mineral assemblages are used as reference for application of multi-component geothermometry.

Table 1. Secondary minerals identified near Breitenbush Hot Springs. In the "Occurrence" column the letters indicate presence in the CTGH-1 (C), SUNEDCO 58-28 (S), outcrops near Breitenbush (O), and in three shallow boreholes near Austin Hot Springs as described by Boden (1985) (B)

Type	Mineral	Occurrence
Silica	chalcedony	C, S, O
	christobalite	C, S, O, B
	opal	O
	quartz	C, S, O, B
Zeolites	analcime	C, S, O, B
	Chabazite	C, O
	clinoptilolite	C, O
	epistilbite	S,O, B
	erionite	C
	gismondine	O
	heulandite	C, S, O
	laumontite	S,O, B
	levyne	O
	Mesolite	C, O, B
	mordenite	C, S, O, B
	phillipsite	C, O
	scolecite	S,O
	stilbite/stellerite	S,O, B
	thomsonite	C, O
	wellsite	C
	yugawaralite	O
Clays/Mica	celadonite	C, S, O, B
	halloysite	O
	illite	S, O, B
	kaolinite	O
	mixed layer chlorite-smectite	S,O
	mixed layer chlorite-smectite	O
	mixed layer illite-smectite	O
	serpentine-kaolinite	S
	smectite	C, S, O, B
	vermiculite	O
Carbonates	calcite	C, S, O, B
	dolomite	O, B
	siderite	S,O, B
Sulfur	anhydrite	S
	chalcopyrite	S,O
	cinnabar	O
	galena	O
	gypsum	O
	polybasite	O
	pyrite	S,O, B
	sphalerite	O
Iron Oxides	hematite	O, B
	iron oxide	C, S, O
	magnetite	S,O, B
Other	actinolite	O
	adularia	C, O
	Antigorite	B
	apatite(?)	C
	apophyllite	O
	chlorite	S,O, B
	chrysocolla	O
	cordierite	O
	corrensite (?)	S
	epidote	S,O, B
	garnet	O
	hornblende	O
	native copper	C
	sepiolite(?)	S
	talc	O

Heat flow data collected from temperature-gradient wells in the Breitenbush area show an extension of high heat flow from the Cascade crest to the west at the location of Breitenbush Hot Springs (Blackwell and Baker, 1988). The high temperature aquifer associated with this heat flow anomaly was present at a depth of 800 m in the SUNEDCO drill hole at a temperature of approximately 116°C. Below this depth, the temperature gradient data (Figure 3) suggest conductive heat flow to a maximum approximate borehole temperature of 141°C at the bottom of the hole (2,457 m) (Blackwell and Baker, 1988). The maximum recorded borehole temperature of a well installed at the Breitenbush Hot Springs Resort is 116°C recorded in W3 (Figure 10; Blackwell and Baker, 1988). Current surface outflow temperatures from wells are as high as 85°C. Based on the apparent depth of the thermal aquifer and its relationship to local geologic structures, it was posited that the source of the heat was derived from igneous processes beneath the Cascade crest (i.e. near Mount Jefferson). Permeability contrasts between a highly altered zone of the Breitenbush Tuff and the overlying HCG allow movement of thermal water from the east to the west along the Breitenbush anticline, thus producing the observed high heat flow anomaly to the west of the Cascade crest, and providing a theoretical framework for the hot springs (Sherrod and Conrey, 1988).

Several estimates of reservoir temperature have been made by various chemical geothermometers. An estimated reservoir temperature of 174°C based on silica geothermometers was derived in 1982 as part of a large-scale study across the Cascades (Forcella, 1982). A second estimate of 174°C was derived from forced equilibrium with anhydrite (Ingebritsen et al., 1992). A summary of classical geothermometers, including a sulfate isotope geothermometer, resulted in estimates from 129 to 202 °C (Mariner et al., 1993). Multi-component geothermometers produced estimates of 180°C (Pang and Reed, 1998) and 176°C (Spycher et al., 2016). In both cases, Al concentrations were derived by forced equilibrium with microcline. These temperatures were considered reasonable when compared to the anhydrite equilibrium and sulfate isotope data of Mariner et al. (1993).

In addition to these reservoir estimates using geothermometers, an analysis of fluid inclusions found in the SUNEDCO 58-28 and CTGH-1 drill holes determined temperatures ranging from 113 to 232 °C (Bargar, 1994). The majority of fluid inclusion temperatures, particularly those from secondary calcite and anhydrite minerals, were coincident with measured borehole temperatures at the sample depth, suggesting that they had formed in equilibrium with the current geothermal system. Fluid inclusions found in hydrothermal quartz and primary quartz phenocrysts generally showed temperatures greater than the measured borehole temperature at the associated depth (Bargar, 1994).

3. APPROACH

3.1 Field Methods

A total of 13 well samples, 5 spring samples, and 2 river samples were collected from Breitenbush Hot Springs (Figure 2). Sample locations were determined in the field using a handheld GPS unit. Samples from Breitenbush wells and springs were collrected between October 7, 2014 and June 30, 205. A series of samples were collected from the W10 on June 30, 2015 to determine the change in water chemistry with the volume of water extracted.

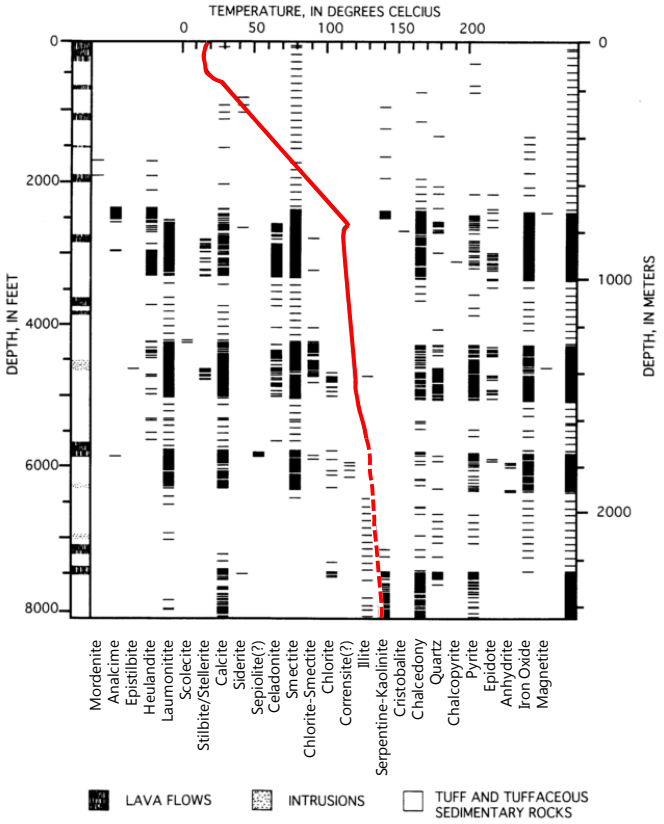

Figure 3. Distribution of hydrothermal minerals with depth in the SUNEDCO 58-28 drill hole. Left column shows the stratigraphic section of rock units encountered. Column on far right shows where the samples were taken. A temperature with depth curve is superimposed on the graph (from Bargar, 1994).

Spring waters found as pools (180° Spring, South Camp Spring) were collected by first observing any bubbles emerging from cracks on the pool bottom to identify the likely point of spring discharge. A Teflon beaker attached to a telescoping polyvinylchloride rod was then placed close to the point of likely discharge and inverted for sample collection. For flowing springs (Iron Spring, No Tobacco Spring, Sulphur Spring), sample bottles were placed directly into the flow path.

Wells W1, W3, and W4 provide water for district heating and/or filling of soaking pools at the Breitenbush Hot Springs Resort. To sample these wells, a fire hose was attached to a discharge outlet and the wells were allowed to purge for at least one well volume prior to sample collection. Wells at Breitenbush Hot Springs are completed as uncased holes in bedrock without filter pack. When the wellhead is opened, well W10 flows under artesian conditions at approximately 19 L/s. A total of six samples were collected from this well at intervals of ~20 to 60 minutes and increasing temperatures of 62, 64, 72, 77.5, 79.5, and 82 °C to identify any changes in water chemistry with additional purging and differing sample temperature. Samples were collected from tubing at a point approximately 7 meters from the wellhead. W14 flows constantly at a rate of approximately 0.06 L/s from the top of the wellhead. Samples were collected directly from the flowing water without purging. Water levels in wells W2, W11, and W12 are below the well casing and thus had to be pumped to the surface. The water level in W12 was high enough in the casing to sample with a peristaltic pump. The low-flow nature of the pump allowed the use of a flow-through cell, which was constantly monitored until parameters stabilized before sample collection. The water levels in W2 and W11 were too deep for the use of a peristaltic pump. Well W2 was purged for three well volumes and then sampled through tubing attached to an aboveground Toyota water pump. Well W11 was purged for approximately one well volume using a submersible pump attached to a 2.5-cm hose.

At each sample location, measurements of temperature, specific conductance, electrical conductivity, oxidation-reduction potential (ORP), pH, and dissolved oxygen content were made using a calibrated YSI multimeter. For well samples, water was pumped via a hose into a YSI flow-through cell in which readings were collected. For waters in excess of 40°C, the water was first sent through a heat exchanger constructed of coiled stainless steel tubing surrounded by ice in a cooler in order to cool the water to temperatures appropriate for use with the YSI meter. For spring samples, either the probe was inserted directly into the spring or, for spring waters exceeding 40°C, readings were collected in filled containers which had been allowed to cool. ORP measurements were made with a combination platinum electrode with a Ag/AgCl (4M KCl) reference electrode calibrated using ZOBELL solution. pH was calibrated in the field immediately prior to sampling using pH 4, 7, and 10 buffer standards. Alkalinity was determined in the field using a HACH digital titrator equipped with either a 0.160 or 1.600 N H_2SO_4 cartridge and bromcresol green-methyl red to indicate the total alkalinity endpoint. Two alkalinity measurements were made at each location and the average of the two was tabulated. Samples for ion analyses

were filtered through a 0.45 μm polyethersulfone membrane syringe filter and collected into acid washed, low-density polyethylene bottles. Samples retained for cation analysis were acidified in the field to < pH 2 using trace-metal grade HNO_3. Samples for anion, isotope and laboratory pH and alkalinity analyses were filled with every effort to eliminate air bubbles in the headspace. All samples were transported to the laboratory in an ice-filled cooler.

3.2 Laboratory Methods

Total alkalinity was measured at Portland State University within 48-hours of sample collection by titrating 0.05 N HCl into 50 ml of sample while recording pH values every 0.1 ml until reaching a pH well below the HCO_3^- inflection point. Once sufficient data was recorded, the alkalinity value was calculated using the Gran Function (Gran, 1952). Alkalinities are reported as milligrams per liter (mg/L) of $CaCO_3$ and HCO_3^-. Samples were analyzed for major anions (Cl, F, Br, PO_3^- NO_3^-, and N^-) using a Dionex IC25 ion chromatograph equipped with a conductivity detector. Concentrations were determined using a suite of external standards prepared from commercial, NIST-traceable stock solutions with ion concentrations ranging from 0.1 to 200 ppm. Large dilutions of split samples were necessary to measurement of the Cl concentrations of some water samples. Major, minor, and trace cation concentrations were analyzed using an Agilent 720 axial ICP-OES. Calibration was performed using up to 15 external calibration standards prepared from commercial NIST-traceable stock standards. Although silica was analyzed via ICP-OES, silica concentrations were also measured for thirteen select (unacidified) samples using the molybdate-yellow method with transmittance read at 410 nm on a Beckman Coulter DU 730 UV/V is Spectrophotometer. The relative percent differences between methods ranged between 1.8 and 15.2% with an average of 5.2%. Samples were also submitted to the Northern Arizona University Stable Isotope Laboratory for analysis of deuterium and stable oxygen isotopes (i.e. ^{18}O and ^{16}O) using a LGR Liquid Water Isotope Analyzer DLT-100.

3.3 Geothermometry

Geothermometry was interpreted with the Reservoir Temperature Estimator (RTEst) software package (Palmer, 2015). RTEst minimizes the weighted sum of squares of the saturation indices of a user-selected set of minerals believed to be at equilibrium within the reservoir by adjusting the temperature, fugacity of CO_2 (fCO_2), and mass of water. RTEst uses the React module in The Geochemist's Workbench (GWB) (Bethke and Yeakel, 2011) to do the geochemical calculations while using PEST (Doherty, 2005, 2013) to perform the optimization calculations. For the weights, we used the inverse variance method that is based on the conditional variance of the saturation index. For mineral k, this conditional variance ($s^2_{SI_k}$) is approximately

$$s^2_{SI_k} \approx \left(\frac{1}{\ln(10)}\right)^2 \left[\sum_{i=1}^{nc} v_{ik}\left(\frac{s_{C_i}}{C_i}\right)^2\right] \quad (1)$$

where v_{ik} is the stoichiometric coefficient of the ith basis species in the kth mineral phase and s_{C_i} / C_i is the coefficient of variation of the concentration of the ith basis species, (i.e., the analytical uncertainty in the reported concentration). More details can be found Palmer (2015) and Palmer et al. (2014).

For the calculations reported here, we used the thermo.tdat thermodynamic database associated with The Geochemist's Workbench. Optimized parameters were reservoir temperature and the logarithm CO_2 fugacity. Adding water to the system to account for steam formation was not done as initial runs indicated that including water as an optimization parameter lead to large parameter uncertainties. Several mineral assemblages were considered for the multicomponent geothermometry calculations based on previously reported mineral distributions.

4. RESULTS

4.1 Analytical Results

Field temperatures and pH of the springs and wells ranged from 16 to 82°C and 6.9 to 9.30. With the exception of the two river samples, and wells W12, and W11, all of the samples plotted distinctly as Na-Cl waters. W12 plots as a Na-HCO_3^- water and W11 is somewhat in between. This separation of W11 and W12 from the others is consistent with total dissolved solids values of less than 400 mg/L for W11 and W12 compared to values greater than 2,000 mg/L for the remainder of the samples. These data indicate a potential shallow, more recently recharged source for W12. W11 may represent a mixture between non-thermal background water (W12) and the thermal reservoir water. Fractions of thermal water in W11 based on Cl and Br concentrations are 3.9 and 4.1%, respectively. Mixing of thermal and nonthermal waters in W11 is further supported by maximum down-hole temperature of 39°C. The upstream sample is a Na-HCO_3 water while the downstream sample is between the Na-HCO_3 and Na-Cl end-members, reflecting input of thermal water into the stream.

W2 and W14 show similarities to the majority of the other thermal water samples collected from Breitenbush in some dissolved ion concentrations (Cl^-, F^-, SO_4^{2-}, Ca^{2+}, and Na^+) and differences in others (notably SiO_2, HCO_3^-, Mg^{2+}, K^+, As, and Mn^{2+}). The similarity in the conservative Cl^- ion in particularly suggests that the waters may have originated from a similar thermal source as the other waters. Their depletion in other ions suggests that they may have experienced more shallow mineral precipitation than other wells and springs. W2 and W14 had water temperatures of 17.6 and 29 °C during sampling, both of which are much cooler than the other waters with a thermal signature. These cooler temperatures could be due to relatively slower flow paths, which would provide more time for mineral precipitation between the reservoir and the surface and thus explain the difference in water chemistry. The differences between the average concentrations of Mg^{2+}, K^+, and SiO_2 in W1, W3, W4, and the hot springs with the measured concentrations of Mg^{2+}, K^+, and

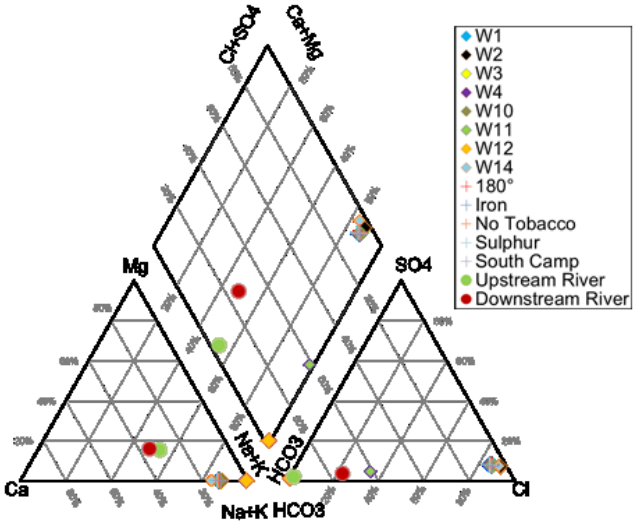

Figure 4. Piper diagram of Breitenbush samples. Note that W12 and W11 are the only non-river samples that plot outside of the Na-Cl water quadrant. The majority of the samples overprint each other near the tip of the Na-Cl quadrant. Wells are depicted with diamonds, springs are depicted with crosses, and stream samples are depicted with circles.

SiO_2 in W2 are 0.030 mmol, 1.2 mmol, and 2.1 mmol, respectively. The differences between the average concentrations of Mg^{2+}, K^+, and SiO_2 in W1, W3, W4, and the hot springs and the measured concentrations in W14 are 0.023 mmol, 0.91 mmol, and 1.3 mmol, respectively. The ratios of these differences (W2/W14) are 0.77, 0.76, and 0.62. The consistency in these ratios suggests that there is also consistency in the minerals precipitated during ascent, with the waters in W2 having undergone more precipitation than the waters in W14.

Water from W10 was sampled multiple times as it continuously flowed from the well head after opening the valve. While nearly all of the dissolved constituents remained constant as water was pumped, Fe and Al generally decreased with the extracted temperature (Figure 5). The Al concentration approaches the average concentration of Al in the springs (5.9 ±2.0) as the temperature approaches 82°C. This result suggests that there may be some bias in the Al concentrations obtained from the wells. In addition, it is possible that some of the lower Al concentrations in the springs are biased due to the coprecipitation of Al in $Fe(OH)_3$ as a result of oxidation of Fe(II) at the discharge. For these reasons, Al concentrations for the geothermometric calculations were calculated based on the assumptions of equilibrium with K-feldspar. This "fixed-Al" approach was introduced by Pang and Reed (1998) and has been used by many researchers. The use of K-feldspar to derive Al concentrations has been applied in other multi-component geothermometry investigations, including at Breitenbush Hot Springs (Spycher, 2016). In addition, adularia was reported in a sample collected from CTGH-1 at a depth of 1,293 m (Bargar, 1988), showing that it is present in the geothermal system.

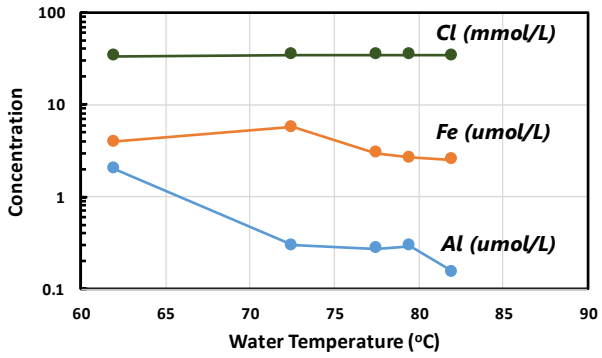

Figure 5. Fe, Al and Cl concentrations from W10 as a function of extraction temperature.

4.2 Geothermometry Results

The multicomponent geothermometry calculations were made with the RTEst software package using a mineral assemblage based on secondary minerals identified in the CTGH-1 and SUNEDCO drill holes (Bargar, 1994; Bargar, 1988; Barger and Oscarson, 1997). The set of minerals used for these calculations was chalcedony, calcite, heulandite, and mordenite-K with Al concentrations from assumed equilibrium with K-feldspar. Calcite, chalcedony and heulandite were identified in drill holes CTGH and SUNEDCO 58-28, as well as in outgroup samples in the area (Barger and Oscarson, 1997). They were also observed during drilling of W10 (Waibel, 1983). Only two

occurrences of mordenite are reported for the SUNEDCO 58-28 drill hole (Bargar, 1994), but it occurs in outcrop samples in the area and is described as abundant in drill hole CTGH-1. Mordenite has also been observed in other localities in the Cascades of northern Oregon including the Mount Hood area and the Newberry Volcano area (Barger and Oscarson, 1997). Bargar (1994) states that, "mordenite is a late hydrothermal mineral deposited in open spaces of fractures and vugs together with heulandite and chalcedony". The chosen assemblage may thus represent the current geothermal system. The average and standard deviations of saturation indices ($\log_{10}(Q/K_{sp})$) from all of the springs and wells W1, W2, and W3 for these minerals are all within 1 standard deviation (based on the conditional variance, Eq.(1) of the expected uncertainty of the equilibrium state given the stoichiometry and the analytical uncertainty for each mineral (Figure 6).

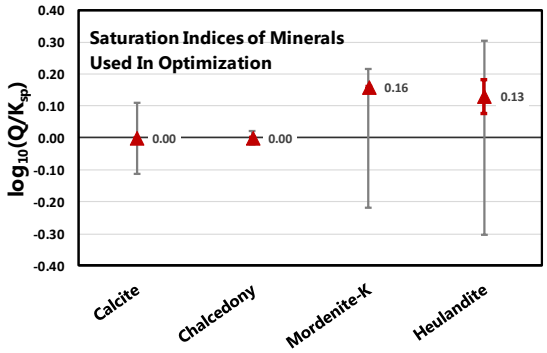

Figure 6. Saturation indices of mineral used in the optimization using RTEst. The triangles are the mean value over the set of reservoir wells and springs. The red vertical bars are the standard deviations about the mean optimized saturation indices. The vertical grey bars are the standard deviations in the equilibrium state ($\log_{10}(Q/K_{sp})$ = 0.0) based on the stoichiometry and analytical uncertainty (see Palmer, 2015).

The results of the computed aqueous geochemical parameters from the multicomponent geothermometric calculations are summarized in Figure 7. The calculated reservoir temperatures for the springs and Wells W1, W3, and W4 are fairly consistent (137.0 ±2.0°C). Samples W10-82, W14, and W2 have temperatures of 129.6, 90.3, and 41.0°C, respectively, and are statistically different from the mean at the 95% significance level. This result together with the element ratios discussed in the previous section suggest that the water in these wells is derived from thermal water that has cooled and re-equilibrated with the same mineral suite. Because the estimated reservoir temperatures from the springs and wells W1, W2, and W3 are so similar to one another, we consider these samples, the "reservoir samples", to be representative of the reservoir water and calculate all additional reservoir parameters from this set of samples.

For the reservoir samples, $\log_{10}(f(CO_2))$ (-0.07 ±0.08) and pH (6.06±0.05) are also relatively constant. W2 and W14 show significant depletion in CO_2 and increases in pH relative to the reservoir samples while f(CO2) and pH for W10-85 are not significantly different from the reservoir samples. The mean of calculated Al concentrations for the reservoir samples (9.6 ±0.5 ug/L) is consistent with the mean of measured concentrations (8.9 ±4.6 ug/L). The calculated Al concentrations for W10-82, W14, and W2 are all significantly greater than the mean value for the reservoir samples at the 95% significance level. The calculated redox potential for the reservoir samples (0.07 ±0.15 volts) excludes the 180° spring data since it values exceeds the 95% confidence interval and may have been contaminated with O_2 during sample collection. The redox potentials for W10-82, W14, and W2 are not significantly different from the reservoir samples.

In addition to the minerals used in the optimization, we looked at the mineral saturation indices of selected minerals under the optimized conditions for each of the wells. The results are summarized in Figure 8. The calculations suggest that the reservoir waters are equilibrated with laumontite, illite, and kaolinite, minerals specifically identified in drill cuttings from SUNEDCO 58-28 drill hole and in outcrop samples. Several smectites including beidellite-H, -K, -Mg, -Ca appear to be either equilibrated or supersaturated in the calculated reservoir waters indicating a thermodynamic potential for their formation. This result is consistent with "smectites" reported in the SUNEDCO and CTGH-1 drill holes, and outcrop samples. The key mica identified in the SUNEDCO 58-28 drill hole was celadonite and it is also reported in CTGH-1 and outcrop samples. While this phase is not included in the thermodynamic database that we used, our calculations indicate the posited reservoir water is equilibrated with paragonite and illite and supersaturated with muscovite, which are structurally similar micas. The supersaturated condition with respect to quartz, goethite and epidote is consistent with their observation in the formation. Other minerals with which the calculated reservoir water may be equilibrated are fluorite (CaF_2), pyrophyllite ($Al_2Si_4O_{10}(OH)_2$), and petalite ($Li_2Al_2Si_8O_{20}$), though their occurrences in the area have not been documented. The posited reservoir fluid appears to be at equilibrium or supersaturated with clinoptilolite (-K, -Ca); although this phase is not reported in the list of identified minerals from the SUNEDCO 58-28 drill hole or the outcrop samples, it is reported in the CTGH-1 drill hole samples. The clinoptilolite XRD pattern is nearly identical to that of heulandite (Ming and Mumpton, 1989) so it is possible that some of the reported heulandite is actually clinoptilolite. Minerals reported in the area for which we did not find a thermodynamic potential for their formation include the zeolite analcime ($NaAlSi_2O_6{\cdot}H_2O$) (SI = -0.78 ±0.05) and siderite ($FeCO_3$). One possible explanation for the discrepancy for analcime is substitution in the idealized analcime structure which could have altered its solubility product. There is a solid solution between the pure Na end-member (analcime) and the Ca end-member (wairakite). Electron microprobe analysis of individual crystallites (Bargar and Oscarson, 1997) suggest that both analcime and wairakite are present in the formation. The analcime

sample contains approximately 73% Na and 27% (Ca+Mg) while the wairakite samples contain 44-60% (Ca+Mg), 31-43% Na, and 5-15% (K+Ba+Sr). However, the reservoir waters are more undersaturated with respect to pure wairakite than with analcime. Analcime does not appear to be evenly distributed over the reservoir but, with the exception of two samples, seems to concentrated in an interval between 685-765 m depth. For siderite, it is observed that there were only 5 reported occurrences over the 2400 m of the SUNEDCO drill hole. Of those five occurrences, 3 occur at ~220 m depth where the temperature was 45°C.

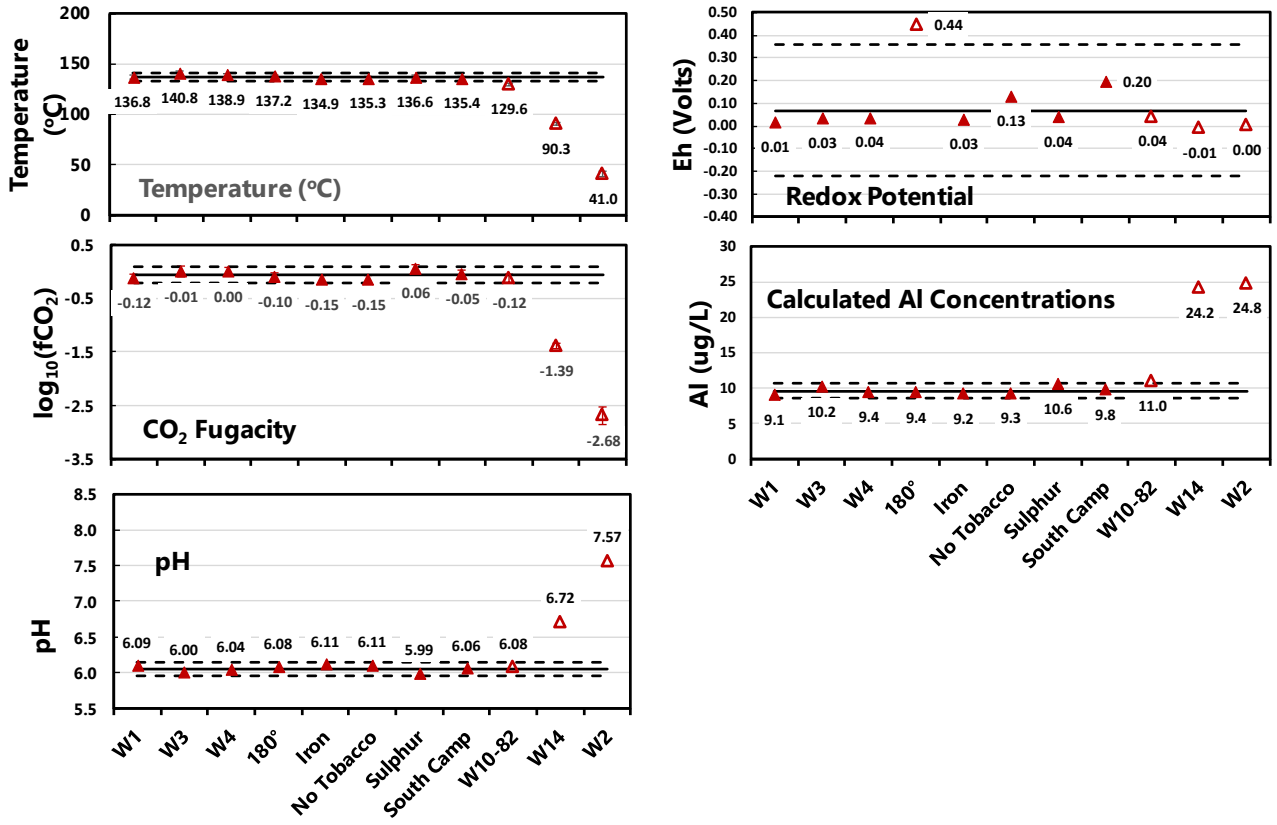

Figure 7. Aqueous geochemical parameters from multicomponent geothermometry calculations using RTEst. The solid horizontal line is the average value of samples with filled symbols while the dashed lines are 95% confidence intervals.

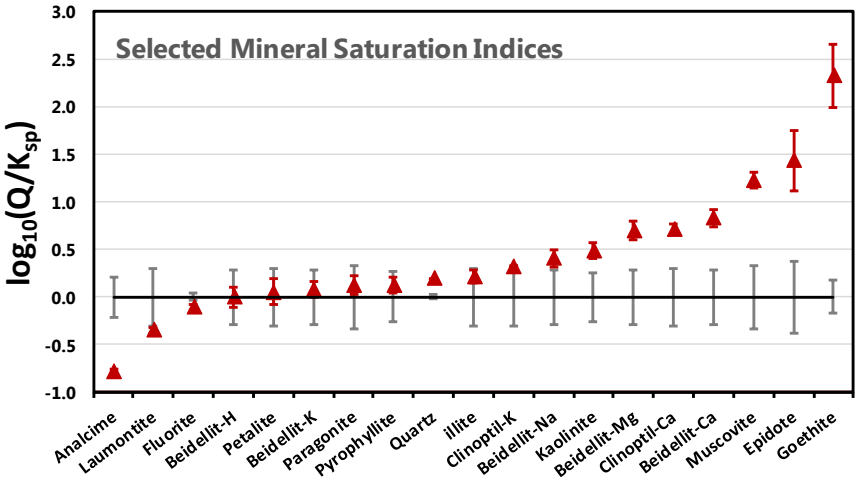

Figure 8. Saturation of selected minerals in the reservoir. Triangles denote the mean value over the reservoir samples and the associated error bars are for 1 standard deviation. The error bars about the saturation line are the standard deviations derived from Eq. (1). The minerals are arranged in increasing order of saturation.

5. DISCUSSION

Past reservoir temperature estimates based on classical geothermometers and a sulfate isotope geothermometer range from 129 to 202°C (Mariner et al., 1993; Ingebritsen et al., 1992). Previous multicomponent geothermometric calculations (Pang and Reed, 1998; Spycher et al., 2016) have suggested temperatures in the range of 176°C to 180°C. These are consistent (if slightly higher) than the median quartz assemblage temperatures determined with GeoT and RTEst (Malkemus, 2016), but much higher than the chalcedony, heulandite, mordenite-K, and calcite temperature estimate of 137 °C. A difficulty with choosing a mineral assemblage that includes quartz, is that the posited reservoir waters are undersaturated with respect to chalcedony. This undersaturation appears to contradict observations from the SUNEDCO drill hole that show that chalcedony occurs more frequently than does quartz. In contrast, if the reservoir waters are equilibrated with chalcedony, they would be supersaturated with respect quartz and a chemical potential for its precipitation would exist.

An additional problem with using quartz in the mineral suite are the resultant Al concentrations that are calculated based on equilibrium with feldspars. Pang and Reed (1998) describe a reservoir estimate of 180°C for Breitenbush Hot Springs. By forced equilibrium with albite, the Al concentrations would be 162 to 189 ug/kg (using GeoT's built-in FixAl feature). Similarly, Spycher et al. (2016) used forced equilibrium with microcline at quartz and anhydrite equilibrium to generate a temperature of 176 °C, which would result in Al concentrations of 81 to 135 ug/kg. These estimates are 9 to 21 times greater than the measured concentrations of 8.9 ±4.6 ug/L. In contrast, our proposed geothermometric model yields Al concentrations of 9.6 ±0.5 ug/L which is similar to the measured concentrations.

Pang and Reed (1998), Spycher et al. (2016), as well as Ingebritsen (1992) and Mariner (1993) have used equilibrium with anhydrite in their estimates reservoir temperatures in the Cascades. However, in the Breitenbush Hot Springs area, anhydrite is only reported in the SUNEDCO 58-28 drill hole and only in two narrow zones between 1792 and 1920 m. Given the relatively rare occurrence of anhydrite in the Breitenbush Hot Springs area, we would not recommend using it for geothermometric calculations.

Our estimated reservoir temperature of 137 ±2°C is also consistent with fluid inclusion data from the SUNEDCO drill hole, which showed a good correlation between measured borehole depth and fluid inclusion temperature (Bargar, 1994; Bargar and Oscarson, 1997). Fluid inclusion data for quartz crystals SUNEDCO 58-28 drill hole and outcrops in the area show wide range of homogenization temperatures from 124 to 294°C while those for calcite and anhydrite range from 120 to 159°C with an average of 135 ± 13°C (Bargar and Oscarson, 1997). More direct evidence to support our reservoir temperature estimate are the recorded borehole temperatures from the SUNEDCO 58-28 drill hole (Figure 3). The temperature increases from ambient air temperature to approximately 115°C at a depth of 680 m and then increases to a maximum of 141°C at 2400 m (Bargar, 1994). This measured temperature is consistent with estimates based on chalcedony mineral assemblages rather than the quartz-based assemblages used in other studies.

6. CONCLUSIONS

The geothermometry of Breitenbush Hot Springs area was interpreted by means of a multicomponent optimization approach using the Reservoir Temperature Estimator (RTEst) software package (Palmer, 2015). Using a mineral assemblage consisting of chalcedony, heulandite, mordenite-K and calcite and deriving Al concentrations from assumed equilibrium with K-feldspar resulted in an average temperature estimate of 137 ±2 °C.

This calculated reservoir temperature is significantly less than the 174 to 180 °C values reported in other multicomponent geothermometric studies (Forcella, 1982; Ingebritsen et al., 1992; Pang and Reed, 1998; Spycher et al., 2016). However, our new estimate shows promise in its consistency in estimated reservoir temperature, CO_2 fugacity (log(fCO2) = -0.06 ±0.07) and pH (6.04 ±0.06). In addition, calculated Al concentrations (9.6 ±0.5 ug/L) are consistent with the measured concentrations (8.9 ± 4.6 ug/L). Most of the reported secondary minerals can be explained by equilibrium or supersaturated states obtained with this model. The estimated reservoir temperature is close to the reported maximum downhole temperature of 141 °C in a deep well located 3 km southeast of the hot springs as well as fluid inclusion data (Bargar, 1994) from the same borehole. Thus, the proposed geothermometric model is consistent with mineralogical, aqueous geochemical, and borehole temperature observations and estimates based on fluid inclusions near the site.

REFERENCES

Arnórsson, S.: Strategy in Geothermal Exploration, Development and Production, in: Arnórsson, S. (Ed.), *Isotopic and Chemical Techniques in Geothermal Exploration, Development and Use: Sampling Methods, Data Handling, Interpretation*. International Atomic Energy Agency, Vienna (2000).

Bargar, K.E.: Secondary Mineralogy of Core from Geothermal Drill Hole Ctgh-1, Cascade Range, Oregon, in: Sherrod, D.R. (Ed.), *Geology and Geothermal Resources of the Breitenbush-Austin Hot Springs Area, Clackamas and Marion Counties, Oregon* (1988).

Bargar, K.E.: Hydrothermal Alteration in the Sunedco 58-28 Geothermal Drill Hole near Breitenbush Hot Springs, Oregon, *Oregon Geology*, **56**, (1994).

Bargar, K.E., Oscarson, R.L.: Zeolites and Selected Other Hydrothermal Minerals in the Cascade Mountains of Northern Oregon, in: 97-100, U.S.G.S.O.F.R. (Ed.), (1997), p. 64.

Blackwell, D.D., Baker, S.L.: Thermal Analysis of Austin and Breitenbush Geothermal Systems, Western Cascades, Oregon, in: Sherrod, D.R. (Ed.), *Geology and Geothermal Resources of the Breitenbush-Austin Hot Springs Area, Clackamas and Marion Counties, Oregon* State of Oregon Department of Geology and Mineral Industries Open-File Report 0-88-5 (1988).

Boden, J.R., 1985. Lithology, hydrothermal petrology, and stable isotope geochemistry of three geothermal exploration drill holes, upper Clackamas River area, Cascade Range, Oregon: Riverside, University of California, unpub. MS thesis, 137 p.

Forcella, L.: Geochemistry of Thermal and Mineral Waters in the Cascade Mountains of Western North America, *Ground Water*, **20**, (1982), 39-47.

Fournier, R.O.: Chemical Geothermometers and Mixing Models for Geothermal Systems, *Geothermics*, **5**, (1977), 41-50.

Gran, G.: Determination of the Equivalence Point in Potentiometric Titrations, *Analyst*, **77**, (1952), 661-671.

Hammond, P.E.: A Tectonic Model for Evolution of the Cascade Range, in: Armentrout, J.M., Cole, M.R., TerBest, H.J. (Eds.), *Cenozoic Paleogeography of the Western United States: Pacific Coast Paleogeography Symposium 3*. Society of Economic Paleontologists and Mineralogists, Los Angeles (1979).

Ingebritsen, S.E., Sherrod, D.R., Mariner, R.H.: Heat Flow and Hydrothermal Circulation in the Cascade Range, North-Central Oregon, *Science*, **243**, (1989), 1458-1462.

Ingebritsen, S.E., Sherrod, D.R., Mariner, R.H.: Rates and Patterns of Groundwater Flow in the Cascade Range Volcanic Arc, and the Effect on Subsurface Temperatures, *Journal of Geophysical Research*, **97**, (1992), 4599-4627.

Keith, T.E.C.: Regional Patterns of Hydrothermal Alteration in the Breitenbush-Austin Hot Springs Area of the Cascade Range Oregon, in: Sherrod, D.R. (Ed.), *Geology and Geothermal Resources of the Breitenbush-Austin Hot Springs Area, Clackamas and Marion Counties, Oregon*, State of Oregon Department of Geology and Mineral Industries Open-File Report 0-88-5 (1988).

Malkemus, D.A.: Geothermometry of Two Cascade Geothermal Systems. Portland State University, Portland, (2016), p. 173.

Mariner, R.H., Presser, T.S., Evans, W.C.: Geothermometry and Water-Rock Interaction in Selected Thermal Systems in the Cascade Range and Modoc Plateau, Western United States, *Geothermics*, **22**, (1993), 1-15.

Ming, D.W., Mumpton, F.A.: Zeolites in Soils, in: Dixon, J.B., Weed, S.B. (Eds.), *Minerals in Soil Environments*. Soil Science of America, Madison, WI (1989).

Palmer, C.D., 2015, Reservoir temperature estimator (RTEst) user's manual. IN: Mattson, E.D., Smith, R.W., Neupane, G., Palmer, D.D., Fujita, Y., McLing, T.L., Reed, D.W., Cooper, C., and Thompson, V.S., 2015, Improved geothermometry through multivariate reaction-path modeling and evaluation of geomicrobiological influences on geochemical temperature indicators: Idaho National Laboratory, INL/EXT-14-33959.

Palmer, C.D., Ohly, S.R., Smith, R.W., Neupane, G., McLing, T., Mattson, E.: Mineral Selection for Multicomponent Equilibrium Geothermometry, *GRC Transactions*, **38**, (2014), 453-460.

Pang, Z.H., Reed, M.H.: Theoretical Chemical Thermometry on Geothermal Waters: Problems and Methods, *Geochimica et Cosmochimica Acta*, **62**, (1998), 1083-1091.

Priest, G.R.: Volcanic and Tectonic Evolution of the Cascade Volcanic Arc, Central Oregon, *Journal of Geophysical Research: Solid Earth*, **95**, (1990), 19583-19599.

Sherrod, D.R., Conrey, R.M.: Geologic Setting of the Breitenbush-Austin Hot Springs Area, Cascade Range, North-Central Oregon, in: Sherrod, D.R. (Ed.), *Geology and Geothermal Resources of the Breitenbush-Austin Hot Springs Area, Clackamas and Marion Counties, Oregon*. State of Oregon Department of Geology and Mineral Industries Open-File Report 0-88-5, Portland (1988).

Spycher, N., Finsterle, S., Dobson, P.: New Developments in Multicomponent Geothermometry, Stanford University, (2016), pp. 1387-1395.

Waibel, A.: An Assessment of Heidgerken Breitenbush Wells 1, 2, and 3, Marion County, Oregon. Columbia Geosciences, (1983), p. 24.